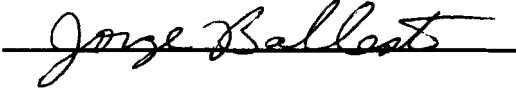


AN ABSTRACT OF THE THESIS OF

Yihong Ding for the Master of Science in Physics presented on July,

1994. Title: Photoelectron Yield Enhancement of Small Graphite and

Silicate Dust Grains. Abstract approved: 

The photoelectron yield for small grains can be much larger than the bulk values, due to the large surface to volume ratio, which leads to an increase in the probability of escape of a photoelectron. Emission of photoelectrons from small interstellar dust grains is believed to be a significant source of heating of interstellar gas. The heating rate is sensitive to the photoelectric yield of the proposed dust grains. A model based on the Mie solution to the vector electromagnetic wave equation in the presence of a sphere is adopted. Unlike the traditional Mie scattering problem, the electromagnetic fields inside the sphere are considered. Previous calculations utilizing the model are extended. In particular, the relationship of the relative photoelectron yield to wavelength and grain size via a complex index of refraction is investigated. Graphite and silicate grains are considered because they are possible components of interstellar dusts. The published values of absolute photoelectric yield for bulk samples are then used to calculate the absolute yield of small dust grains. The use of $\exp(i\omega t)$ and $\exp(-i\omega t)$ time-conventions in this problem are compared.

Photoelectron Yield Enhancement
of
Small Graphite and Silicate Dust Grains

A Thesis presented to
the Division of Physical Sciences
Emporia State University

In Partial Fulfillment of
the Requirements for the Degree
Master of Science

By

Yihong Ding

July, 1994.

THOS
1994
D

Dwayne Beckner
.....
Approved for the Major Division

Jaye N. Vowell
.....
Approved for the Graduate Council

George Ballant
.....
Committee Chairman

R. J. ...
.....
Committee Member

James W. ...
.....
Committee Member

E. ...
.....
Committee Member

Acknowledgments

I would like to express my deepest thanks to Dr. Jorge Ballester for his guidance and supervision in the completion of this research. I would also like to thank Professors James Calvert, Robert Jones and Ron Keith for their helpful advice and encouragement. I gratefully acknowledge support by NASA/JOVE.

Table of Contents

Chapter 1. Introduction.....	1
Chapter 2. Theory.....	5
Chapter 3. Results.....	22
Chapter 4. Conclusions.....	32
References.....	34
Appendix A.....	37
Appendix B.....	53
Appendix C.....	56

List of Tables and Figures

Table 1.....	25
Table 2.....	26
Figure 1.....	27
Figure 2.....	28
Figure 3.....	29
Figure 4.....	30
Figure 5.....	31

Chapter 1

Introduction

The physical properties of the interstellar medium are described by its density, temperature and phase. The density varies from approximately 5×10^3 to more than 1×10^8 particles per cubic meter. The temperature depends on the balance of heating and cooling mechanisms, and varies from 15 to 5×10^5 K. Hydrogen is the most abundant element in the universe and describing the phase consists of stating the predominant form of hydrogen as molecular (H_2), neutral atomic (HI) or ionized (HII). According to the three-phase model of McKee and Ostriker¹, the interstellar gas has four principal components. These are cold (15 K) molecular H_2 , cool (80 K) atomic HI , a warm (8000 K) mixture of HI and HII , and hot (5×10^5 K) ionized HII ^{1,1}.

The interstellar medium is believed to consist of a diffuse hot ionized HII component, the intercloud medium within which are located denser clouds. The so-called diffuse clouds consist of cool atomic HI surrounded by warm HI and HII . Dense molecular clouds are similar to the diffuse clouds but contain a cold molecular H_2 region in the center. The cold molecular H_2 and cool atomic HI regions are separated by a so-called photodissociation region. All these components are maintained by pressure equilibrium. Interstellar clouds contain hydrogen atoms, assorted molecules and dust grains. These clouds evolve and eventually contract into stars. Cloud temperatures of

100 K or more must be the result of energy exchange among the interstellar radiation field, hydrogen gas, molecules and the dust grains within the cloud. Understanding this energy balance within clouds is very important to quantitative theories of interstellar clouds. Research shows that dust grain photoelectron heating may dominate the gas heating of the intercloud medium and diffuse clouds. It is also significant in *HII* regions.

Interstellar grains play an important role in the energy balance within clouds because they are believed to serve as an intermediary in transferring stellar radiant energy or gas chemical energy into the interstellar gas. The three mechanisms which can transfer starlight energy to gas via grains as described by Hollenbach^{1,2} are photoelectron emission, collisions and desorption.

Interstellar gas may be heated as a result of the emission of photoelectrons from grains (Watson)². For grains which lie near stars with significant ultraviolet (UV) fluxes, the UV absorbed by the grains results in the emission of energetic photoelectrons into the gas. At the same time, free electrons may be captured by the grain. The energy of the ejected electrons is determined by the photoelectric emission process, but the energy of the captured electrons is determined by the free electron temperature. Therefore, there is net heating if the ejected electrons carry more energy than the electrons absorbed by the grains.

The gas may be heated by collisions with grains. Deep in the opaque molecular gas associated with a nearby star, starlight is absorbed by grains. Some of this energy is in turn reradiated by the grains, generally in the

infrared part of the electromagnetic spectrum. Some of this energy can be reabsorbed by the grains and cause temperatures to occur in the range of $30-100\text{ K}$. The cooler gas collides with the warm grains and is heated by conduction, while the infrared photons radiated by the warm grains are absorbed by molecules H_2O or atom O in the opaque, molecular gas. Collisions of these excited molecules and atoms transfer the excitation energy to the gas .

Interstellar gas may also be heated by desorption from thermally fluctuating small grains (Duley)³. Gas heating results from the escape of highly vibrationally excited atoms and molecules from small grains following a sudden temperature increase after the absorption of a single photon. Under special circumstances, this process may be of comparable importance to grain photoelectric heating.

The physical process of grain photoelectric heating is based on the absorption of UV photons by grains and the subsequent ejection of energetic electrons into the gas. Calculating the photoelectric emission from very small particles is very complicated, especially for different geometries and charged grains. The sizes and compositions of dust grains are not certain, but a distribution of spherical graphite and silicate grains represents an acceptable model of interstellar dust.⁴ In this research, we use Watson's model and numerical methods to calculate the relative photoelectron yield, for spherical graphite and silicate grains as compared to the bulk values. We then multiply the published values of the photoelectric yield of bulk samples by this factor to calculate the absolute photoelectron yield of small particles.

In Chapter 2, we present the basic theory. This includes Watson's model of photoelectric emission from grains, the Mie solution to the electromagnetic wave equations, and the detailed numerical methods needed. In Chapter 3, our research results, including tables and graphs are presented. In Chapter 4, we discuss our conclusions. In Appendix A we compare the $\exp(i\omega t)$ and $\exp(-i\omega t)$ time-conventions as they relate to Watson's model. Appendix B presents an example of the type of calculation that can be carried out using our results.

Chapter 2

Theory

1. Watson's Model

Watson presents the basic results of his model, but very few details of the calculations. In order to check the final result and obtain some necessary analytical expressions we have reconstructed a complete derivation of Watson's model. The photoelectric yield Y is defined as the number of electrons emitted divided by the number of incident photons. The basic assumption of Watson's model is that the number of electrons excited in any volume element in the solid is proportional to the number of photons absorbed per unit volume at that location. The number of photons absorbed at any location is calculated from the classical distribution of electromagnetic energy within the material. This model is highly simplified, but it will serve as a first approximation.

Consider a plane, monochromatic electromagnetic wave of angular frequency ω incident on a spherical grain of radius a . The electric and magnetic fields \vec{E} and \vec{H} within the grain can be obtained from the Mie solution⁵ of the vector wave equation in spherical coordinates. The number of photons absorbed per unit time inside the grain can be calculated by integrating the Poynting vector $\vec{S} = \vec{E} \times \vec{H}$ over the surface of the grain and dividing by the energy per photon, that is

$$-\int_A \frac{(\vec{\mathbf{S}} \cdot \vec{\mathbf{n}}) dS}{\hbar\omega} = -\int_V \frac{(\nabla \cdot \vec{\mathbf{S}}) dV}{\hbar\omega}. \quad (1)$$

The minus sign accounts for the fact that energy flows into the grain, but the normal vector $\vec{\mathbf{n}}$ points out of the grain at the surface. Gauss' theorem is used to convert the surface integral to a volume integral. It is concluded that $\left(\frac{\nabla \cdot \vec{\mathbf{S}}}{\hbar\omega}\right)$ is the number of photons absorbed per unit volume per unit time at a particular position within the grain.

Photons absorbed by the grain can liberate electrons from individual atoms, but these do not all escape from the grain. In the case of a bulk sample, Pepper⁶ has given a theory which describes the motion of the electron to the surface. The probability for a photoelectron to be emitted from the surface of a bulk solid when light is absorbed at a distance x below the surface is assumed to be $C \exp(-x/L_e)$. L_e is a characteristic distance which is known as the escape length and C is a constant. Both L_e and C can be determined independently from photoemission experiments with bulk matter. The total number of electrons emitted per unit time from a volume of depth x is

$$\int_V \frac{(-\nabla \cdot \vec{\mathbf{S}})}{\hbar\omega} C e^{-x/L_e} dV. \quad (2)$$

Then the bulk yield Y_b is given by

$$Y_b = \frac{\int_V (\nabla \cdot \bar{\mathbf{S}}) C e^{(-x/L_e)} dV}{\int_V (\nabla \cdot \bar{\mathbf{S}}) dV} \quad (3)$$

If there is no magnetic dissipation and the material is isotropic then,

$$Y_b = \frac{\int_V C e^{(-x/L_e)} (\bar{\mathbf{E}}^* \cdot \bar{\mathbf{E}}) dV}{\int_V (\bar{\mathbf{E}}^* \cdot \bar{\mathbf{E}}) dV} \quad (4)$$

A solution of the boundary value problem shows that

$$\bar{\mathbf{E}}^* \cdot \bar{\mathbf{E}} = K e^{(-x/L_a)}, \quad (5)$$

where K is a constant and the absorption length L_a is given by,

$$L_a = \frac{\lambda}{|4\pi \text{Im}(m)|}. \quad (6)$$

where $\text{Im}(m)$ is the imaginary part of the materials' refractive index. In this case Y_b can be calculated analytically . The integral in equation(4) can be written as,

$$Y_b = \frac{\iint_A dydz \int_0^\infty C e^{-x/L_e} \cdot e^{-x/L_a} dx}{\iint_A dydz \int_0^\infty e^{-x/L_a} dx}, \quad (7)$$

where K has been eliminated from the numerator and denominator. Assume that A is the large but finite surface area of the bulk sample. Then

$$Y_b = \frac{\int_0^\infty C e^{-x \left(\frac{L_e + L_a}{L_e L_a} \right)} dx}{\int_0^\infty e^{-x/L_a} dx} = \frac{C \left(\frac{L_e L_a}{L_e + L_a} \right) (e^{-\infty} - e^0)}{L_a (e^{-\infty} - e^0)}, \quad (8)$$

that is

$$Y_b = \frac{C L_e}{L_e + L_a}. \quad (9)$$

Watson has applied the preceding theory to the case of a spherical grain. In a bulk sample, x is a one-dimensional distance. In a small spherical dust grain, the substitution is made $x = a - r$, where a is the radius of the dust grain and r is the radial position within the sphere. If it is assumed that the same constant C applies to spherical grains, then equation (9) may be used

to solve for C in terms of the experimental bulk yield Y_b ,

$$C = \left(\frac{L_e + L_a}{L_e} \right) Y_b. \quad (10)$$

2. Mie Solution

A physical time-harmonic electromagnetic field in a linear, isotropic, homogeneous medium satisfies the vector wave equations,

$$\begin{aligned}\nabla^2 \vec{\mathbf{E}} + k^2 m^2 \vec{\mathbf{E}} &= 0 \\ \nabla^2 \vec{\mathbf{H}} + k^2 m^2 \vec{\mathbf{H}} &= 0,\end{aligned}\tag{11}$$

and the boundary conditions

$$\begin{aligned}\nabla \cdot \vec{\mathbf{E}} &= 0, \\ \nabla \cdot \vec{\mathbf{H}} &= 0,\end{aligned}\tag{12}$$

where k is the wave number and m is the complex index of refraction of the medium.

Now, two vectors are defined as

$$\vec{\mathbf{M}} = \nabla \times (\vec{\mathbf{r}}\varphi)\tag{13}$$

$$\vec{\mathbf{N}} = \frac{(\nabla \times \vec{\mathbf{M}})}{mk},\tag{14}$$

where φ is a solution of the following scalar wave equation

$$\nabla^2 \varphi + m^2 k^2 \varphi = 0.\tag{15}$$

simple substitution shows that if u and v are two solutions of the scalar wave equation and $\vec{\mathbf{M}}_u, \vec{\mathbf{M}}_v, \vec{\mathbf{N}}_u, \vec{\mathbf{N}}_v$ are the derived vector fields, then

Maxwell's equations are satisfied by

$$\begin{aligned}\vec{\mathbf{E}} &= \vec{\mathbf{M}}_v + i\vec{\mathbf{N}}_u \\ \vec{\mathbf{H}} &= m(-\vec{\mathbf{M}}_u + i\vec{\mathbf{N}}_v).\end{aligned}\quad (16)$$

According to Watson² within the sphere, the independent solutions of the scalar wave equation u and v can be expanded as

$$\begin{aligned}u &= \cos\phi \sum_{n=1}^{\infty} mc_n (-i)^n \frac{2n+1}{n(n+1)} P_n^1(\cos\theta) j_n(mkr) \\ v &= \sin\phi \sum_{n=1}^{\infty} md_n (-i)^n \frac{2n+1}{n(n+1)} P_n^1(\cos\theta) j_n(mkr),\end{aligned}\quad (17)$$

Here $P_n^1(\cos\theta)$ is an associated Legendre polynomial and j_n is the spherical Bessel function. The coefficients c_n, d_n can be obtained from the boundary conditions. It should be noted that the general solution of the scalar wave equation should include associated Legendre polynomials of all orders $P_n^l(\cos\theta)$. However, when the incident plane wave is expanded in spherical coordinates its expansion only includes $l = 1$ terms. Therefore, only the $l = 1$ terms are needed for the solution in equation (17). Watson's

research paper includes few details. We want to extend Watson's numerical calculations. The following derivation provides all analytical expressions which are necessary for this purpose.

By introducing the scalar spherical harmonics ⁷

$$Y_{nl} = \sqrt{\frac{(2n+1)}{4\pi n(n+1)}} P_n^l(\cos\theta) e^{i\varphi} \quad (18)$$

v can be written as

$$v = \sum_{n=1}^{\infty} m d_n (-i)^n \sqrt{4\pi \frac{(2n+1)}{n(n+1)}} j_n(mkr) \text{Im}(Y_{n1}). \quad (19)$$

Then

$$\vec{M}_v = \nabla \times (\vec{r}v). \quad (20)$$

The vector spherical harmonics \vec{X} are defined by ⁸

$$\vec{X} = -\frac{i}{\sqrt{n(n+1)}} \vec{r} \times \nabla Y_{n1}. \quad (21)$$

Because the function $\nabla j_n(mkr)$ only has a radial component, then

$$\vec{r} \times \nabla j_n(mkr) = 0. \quad (22)$$

On the other hand,

$$\begin{aligned}
\bar{\mathbf{X}}_n &= -\frac{i}{\sqrt{n(n+1)}} \bar{\mathbf{r}} \times \nabla [\operatorname{Re}(Y_{n1}) + i \operatorname{Im}(Y_{n1})] \\
&= -\frac{i}{\sqrt{n(n+1)}} [\bar{\mathbf{r}} \times \nabla (\operatorname{Re}(Y_{n1}))] + \frac{1}{\sqrt{n(n+1)}} [\bar{\mathbf{r}} \times \nabla (\operatorname{Im}(Y_{n1}))] \\
&= \bar{\mathbf{X}}_{nr} + \bar{\mathbf{X}}_{ni}.
\end{aligned} \tag{23}$$

We have defined \mathbf{X}_{nr} and \mathbf{X}_{ni} by

$$\bar{\mathbf{X}}_{nr} = -\frac{i}{\sqrt{n(n+1)}} [\bar{\mathbf{r}} \times \nabla (\operatorname{Re}(Y_{n1}))] \tag{23.1}$$

$$\bar{\mathbf{X}}_{ni} = \frac{1}{\sqrt{n(n+1)}} [\bar{\mathbf{r}} \times \nabla (\operatorname{Im}(Y_{n1}))]. \tag{23.2}$$

Then

$$\bar{\mathbf{M}}_v = \sum_{n=1}^{\infty} m d_n (-i)^n \sqrt{4\pi(2n+1)} j_n(mkr) \bar{\mathbf{X}}_{ni}. \tag{24}$$

Similarly,

$$\bar{\mathbf{N}}_u = \frac{1}{k} \sum_{n=1}^{\infty} \left\{ c_n (-i)^{n+1} \sqrt{4\pi(2n+1)} \nabla \times [j_n(mkr) \bar{\mathbf{X}}_{nr}] \right\} \tag{25}$$

The vector spherical harmonics $\bar{\mathbf{X}}_n$ has

$$\int_0^{4\pi} \bar{\mathbf{X}}_n^* \cdot \bar{\mathbf{X}}_{n'} d\Omega = \begin{cases} 1, & (n = n') \\ 0, & (n \neq n') \end{cases} \quad (26)$$

It can be shown that

$$\int_0^{4\pi} \bar{\mathbf{X}}_{nr}^* \cdot \bar{\mathbf{X}}_{n'r} d\Omega = \begin{cases} 1, & (n = n') \\ 0, & (n \neq n') \end{cases}, \quad (27)$$

$$\int_0^{4\pi} \bar{\mathbf{X}}_{ni}^* \cdot \bar{\mathbf{X}}_{n'i} d\Omega = \begin{cases} 1, & (n = n') \\ 0, & (n \neq n') \end{cases}. \quad (28)$$

On the other hand,

$$\begin{aligned} \bar{\mathbf{E}}^* \cdot \bar{\mathbf{E}} &= (\bar{\mathbf{M}}_v + i\bar{\mathbf{N}}_u)^* \cdot (\bar{\mathbf{M}}_v + \bar{\mathbf{N}}_u) \\ &= \bar{\mathbf{M}}_v^* \cdot \bar{\mathbf{M}}_v - i\bar{\mathbf{M}}_v \cdot \bar{\mathbf{N}}_u^* + i\bar{\mathbf{N}}_u \cdot \bar{\mathbf{M}}_v^* + \bar{\mathbf{N}}_u \cdot \bar{\mathbf{N}}_u \end{aligned} \quad (29)$$

Therefore,

$$\begin{aligned} \int_V (\bar{\mathbf{E}}^* \cdot \bar{\mathbf{E}}) dV &= \int_0^a r^2 dr \int_0^{4\pi} (\bar{\mathbf{E}}^* \cdot \bar{\mathbf{E}}) d\Omega \\ &= \int_0^a r^2 dr \int_0^{4\pi} \left(\bar{\mathbf{M}}_v^* \cdot \bar{\mathbf{M}}_v - i\bar{\mathbf{M}}_v \cdot \bar{\mathbf{N}}_u^* + \right. \\ &\quad \left. i\bar{\mathbf{N}}_u \cdot \bar{\mathbf{M}}_v^* + \bar{\mathbf{N}}_u \cdot \bar{\mathbf{N}}_u \right) d\Omega \end{aligned} \quad (30)$$

The integral relations for vector spherical harmonics is used, then

$$\int_0^{4\pi} \vec{M}_v^* \cdot \vec{N}_u d\Omega = \int_0^{4\pi} \vec{N}_u^* \cdot \vec{M}_v d\Omega = 0, \quad (31)$$

and ²

$$\int_0^{4\pi} \vec{M}_v^* \cdot \vec{M}_v d\Omega = 4\pi |m|^2 \sum_{n=1}^{\infty} |d_n|^2 (2n+1) j_n^*(mkr) \cdot j_n(mkr), \quad (32)$$

$$\int_0^{4\pi} \vec{N}_u^* \cdot \vec{N}_u d\Omega = 4\pi \sum_{n=1}^{\infty} |c_n|^2 (2n+1) \left\{ m^2 |j_n^*(mkr) \cdot j_n(mkr) + \frac{1}{k^2 r^2} \frac{\partial}{\partial r} \left[r j_n^*(mkr) \frac{\partial}{\partial r} (r j_n(mkr)) \right] \right\} \quad (33)$$

Using equation (24) and (25), Y' can be written as,

$$Y' = \frac{C \int_0^a e^{-(r-a)/L} \left[\int_0^{4\pi} (\vec{M}_v^* \cdot \vec{M}_v + \vec{N}_u^* \cdot \vec{N}_u) d\Omega \right] r^2 dr}{\int_0^a \int_0^{4\pi} (\vec{M}_v^* \cdot \vec{M}_v + \vec{N}_u^* \cdot \vec{N}_u) d\Omega r^2 dr}. \quad (34)$$

Using the result of Pepper,⁶ if the material making up the bulk is the same as that of the small spherical particle, then Y'/Yb is independent of C . Thus the photoyield enhancement for a sphere of radius a as compare to the bulk material can be calculated from the following ratio

$$\frac{Y'}{Y_b} = \frac{(L_e + L_a) \int_0^a e^{-(a-r)/L_e} \left[\int_0^{4\pi} (\tilde{\mathbf{M}}_v^* \cdot \tilde{\mathbf{M}}_v + \tilde{\mathbf{N}}_u^* \cdot \tilde{\mathbf{N}}_u) d\Omega \right] r^2 dr}{L_e \int_0^a \left[\int_0^{4\pi} (\tilde{\mathbf{M}}_v^* \cdot \tilde{\mathbf{M}}_v + \tilde{\mathbf{N}}_u^* \cdot \tilde{\mathbf{N}}_u) d\Omega \right] r^2 dr}. \quad (35)$$

3. Numerical Calculation Method

In order to obtain values of Y_a / Y_b , the coefficients c_n, d_n must be calculated. The formulas are different depending on which kind of time-conventions is used. The following results are obtained using the $\exp(i\omega t)$ time-convention. The use of the $\exp(i\omega t)$ and $\exp(-i\omega t)$ conventions are compared in Appendix A.

A discussion of numerical methods which may be adapted to our problem is given by Bohren and Huffman.¹⁰ From the boundary conditions satisfied by the electromagnetic field, the coefficients c_n, d_n are given by⁹,

$$c_n = \frac{i}{m\psi_n(mx) \{ [D_n(mx) / m + n / x] \zeta_n(x) - \zeta_{n-1}(x) \}} \quad (36)$$

$$d_n = \frac{i}{\psi_n(mx) \{ [mD_n(mx) / m + n / x] \zeta_n(x) - \zeta_{n-1}(x) \}} \quad (37)$$

Where the logarithmic derivative $D_n(x) = \psi'_n(x) / \psi_n(x)$ is introduced, $\psi_n(x)$ and $\zeta_n(x)$ are Ricatti-Bessel functions, and m is still the material's complex index of refraction. The details of this calculation are shown in Appendix A. The reason for writing these expressions using D_n is that D_n satisfies the following backward recurrence relation¹⁰

$$D_{n-1}(x) = \frac{n}{x} - \frac{1}{D_n(x) + \frac{n}{x}} \quad (38)$$

From the above D_{n-1} and D_n function, the following result can be obtained that: if e_n is the error in D_n , and the error in D_{n-1} generated from the above recurrence relation is e_{n-1} , then $e_{n-1} \ll e_n$. Thus, beginning with a coefficient D_n where n is larger than the number of terms required for convergence, more accurate lower-order logarithmic derivatives can be generated by the downward recurrence. The FORTRAN program PE-DING.FOR which performs this calculation process is listed in Appendix C.

On the other hand, in order to obtain the numerical value of c_n , d_n , Ricatti-Bessel functions $\psi_n(x)$ and $\zeta_n(x)$ must be calculated. The definitions of Ricatti-Bessel functions are

$$\begin{aligned} \psi_n(x) &= xj_n(x) \\ \zeta_n(x) &= xh_n(x), \end{aligned} \quad (39)$$

where $j_n(x)$ and $h_n(x)$ are the Spherical Bessel and Hankel functions which are defined from the ordinary Bessel and Hankel functions J and Y ,

$$j_n(x) = \sqrt{\frac{\pi}{2x}} J_{n+\frac{1}{2}}(x),$$

$$y_n(x) = \sqrt{\frac{\pi}{2x}} Y_{n+\frac{1}{2}}(x), \quad (40)$$

The Hankel functions of the first and second type are defined by¹¹

$$h_n^{(1)}(x) = j_n(x) + iy_n(x), \quad (41)$$

$$h_n^{(2)}(x) = j_n(x) - iy_n(x), \quad (42)$$

Which kind of Hankel function should be used depends on which time-convention is used in the calculation. In this research the $\exp(i\omega t)$ time-convention is used, therefore $h_n^{(2)}(x)$ was used throughout the calculation.

A detailed explanation for this choice is given in Appendix A.

The calculation of Ricatti-Bessel functions has been difficult because of the instability of the generation of Bessel functions of complex argument. A downward recurrence method was used in calculations beginning with an arbitrary starting value for the two initial high orders, and renormalizing after reaching the known zeroth-order Ricatti-Bessel function

$$\psi_0(x) = \sin(x), \quad (43)$$

For y_n upward recurrence is stable beginning with

$$y_{-1}(x) = \frac{\sin(x)}{x}$$

$$y_0 = -\frac{\cos x}{x}, \quad (44)$$

any order of y_n may be calculated. In the mean time,

$$\begin{aligned} \zeta_n(x) &= xh^{(2)}_n(x) \\ &= x(j_n(x) - iy_n(x)) \\ &= \psi_n(x) - ixy_n(x) \end{aligned} \quad (45)$$

Using the recurrence formula for spherical Bessel functions ¹²:

$$\frac{2n+1}{x} j_n(x) = j_{n-1}(x) + j_{n+1}(x), \quad (46)$$

$\zeta_n(x)$ can be obtained from known numerical methods.

Unfortunately, there are no numerical values for c_n , d_n available in the literature. However, the scattering coefficients a_n , b_n are given by Bohren and Huffman ⁹. Therefore, the only way to check if these results are correct is to produce a_n , b_n using the same method as calculating c_n , d_n in this research. The results obtained agree with the published values. More details are given by Shi. ¹³

Substituting $z = mkr$ in equations (32) and (33), and using the recurrence relations (38), (39) and (46), the relative photoelectron yield Y/Y_b can be written as

$$\frac{Y'}{Y_b} = \frac{(L_e + L_a) \int_0^a e^{-(r-a)/L_e} F(r) 4\pi r^2 dr}{L_e \int_0^a F(r) 4\pi r^2 dr},$$

where

$$F(r) = \frac{1}{k^2 r^2} \sum_{k=1}^{\infty} (2n+1) |j_n(z)|^2 \times \left\{ |c_n|^2 \left[|D_n|^2 + \frac{n(n+1)}{|z|^2} \right] + |d_n|^2 \right\}$$

(47)

This expression for $F(r)$ can be calculated numerically. By determining the convergence of the series by iteration or using Wiscomb's formula, the termination of the calculation of $F(r)$ can be obtained. In the FORTRAN program PE-DING.FOR, the termination is based on Wiscomb's formula¹⁴..

More details are again given by Shi.^{13.5}

Chapter 3

Results

The numerical method is used in the FORTRAN program PE-DING. We have used this program to calculate the photoelectron yield enhancement for small dust grains. We have used these results to calculate the absolute photoelectron yield using the published bulk sample's photoelectron yield values. The complete program is shown in Appendix C.

Table 1 presents results of the PE-DING.FOR program. The input parameters are from Watson². These results are compared with that of Watson's in Table 2. Our results are almost identical to Watson's. Watson didn't give the complete results for $m=0.71-0.018i$, possibly because of the small imaginary part of m compared to the real part. In our calculations we have noticed that these same values are very difficult to calculate, because the program takes much more time.

Watson's results have been extended by including more wavelengths, grain sizes, and realistic values for the complex index of refraction from Draine and Lee.⁴ These calculations suggest some interesting features. It should be noticed that the size of a dust grain should be compared to the wavelength of incident light. For example, a grain with a radius of 100 \AA is a small dust grain compare to a wavelength of 2000 \AA , but it can not be seen as a small grain when the wavelength is 150 \AA . In fact, a dust grain with a radius of 5000 \AA can be thought as a bulk, because the most important

photon wavelengths in this research are between 912 \AA to 1500 \AA . Grain sizes from 20 \AA to 5000 \AA are used in this research. The reason for this range is that absorption by interstellar hydrogen cuts off this light field at 912 \AA and photons with wavelengths beyond 1500 \AA have small photoelectron yields. Nevertheless, photoelectron yield enhancement of photon wavelengths from 227.9 \AA to 10000 \AA are also calculated. Several figures are presented. Figure 1, 2, 3 are the results from graphite and silicate grains.

The complex index of refraction depends on wavelength. The imaginary part of complex index of refraction is more important to photoelectron yield, for it affects the photon's absorption length. When the absorption length is small, more absorbed photons will be distributed in the region near the grain's surface, therefore, photoelectrons are more easily produced and emitted in this case. When the absorption length is large, photons are absorbed deep in the material, and produce fewer photoelectrons.

Graphite and silicate grains are considered. In the case of graphite, the average photoelectron yield is presented in the final result, because the polarization is considered. The direction of incident light can be separated into two components: one is parallel to the grain's axis, another is perpendicular to it. The final photoelectron yield comes from assuming one-third parallel yield and two-thirds perpendicular yield.

Figure 1 and 2 are graphite yield enhancement. Radius of this dust grain is 100 \AA and 1000 \AA . Both the complex index of refraction and the

photoelectron yield enhancement are shown in the figures. In the region, wavelength smaller than 5000 \AA , the absolute photoelectron yield E_a displays oscillations as a function of complex index of refraction m and wavelength. When the wavelength is larger than 5000 \AA , the photoelectron yield enhancement increases with the wavelength. It supports the assumption that small size effects can play an important role. The similar conclusion can be obtained from figure 3, which is for silicate grains. For the most interesting wavelength region, 912 \AA to 1500 \AA , certain important results can be obtained. Figure 4 and Figure 5 present the behavior of various sizes of graphite and silicate dust grains. The radii are from 20 \AA to 5000 \AA . These figures clearly show that for a given wavelength the absolute photoelectron yield decreases as the grain's radius increases. Relative photoelectron yield is always greater than one, indicating that the small grain's photoelectron yield is greater than that of a bulk sample. The absolute photoelectron yield can be obtained by using the photoelectron yield enhancement from this numerical method times published bulk yield values. The results are shown in Figure 4 and Figure 5. When radii become large, the relative photoelectron yields are closer to one, because the dust grains are more like bulk material.

RAD (A)	WAVEL (A)	m=1.4-0.81i		m=2.5-1.0i		m=0.71-0.018i	
		Le=10 A	Le=100 A	Le=10 A	Le=100 A	Le=10 A	Le=100 A
100	500	1.60	1.204	1.23	1.105	57.91	18.52
	1000	2.67	1.57	2.14	1.42	110.61	35.94
	1250	3.27	1.77	2.64	1.58	137.43	44.68
	2000	5.08	2.35	4.14	2.05	218.49	70.93
	3000	7.50	3.13	6.10	2.68	326.99	105.96
250	500	1.23	1.09	1.07	1.03	28.86	14.32
	1000	1.50	1.27	1.17	1.12	54.48	27.72
	1250	1.66	1.37	1.24	1.18	66.16	34.17
	2000	2.32	1.76	1.78	1.51	101.13	53.51
	3000	3.38	2.34	2.69	1.99	148.95	79.5
500	500	1.15	1.06	1.05	1.02	17.16	10.53
	1000	1.25	1.14	1.08	1.04	30.57	19.92
	1250	1.30	1.18	1.09	1.06	37.72	24.81
	2000	1.52	1.37	1.18	1.15	57.22	38.57
	3000	1.88	1.66	1.37	1.34	81.28	56.11

Table 1. Relative photoelectron yield E_a calculated by using input parameters from Watson. a is the grain radius. L_e is the electron escape length. m is the index of refraction.

RAD (A)	WAVEL. (A)	m=1.4-0.81i		m=2.5-1.0i		m=0.71-0.018i	
		Le=10 A	Le=100 A	Le=10 A	Le=100 A	Le=10 A	Le=100 A
100	500	1.61	1.21	1.23	1.11	57.9	18.5
	1000	2.7	1.58	2.14	1.42	111	35.9
	1250	3.31	1.78	2.64	1.58	137	44.6
	2000	5.14	2.37	4.14	2.05		
	3000	7.59	3.15	6.1	2.68		
250	500	1.23	1.09	1.07	1.03	28.9	14.3
	1000	1.51	1.27	1.17	1.12	54.5	27.7
	1250	1.68	1.38	1.24	1.18	66.2	34.7
	2000	2.35	1.78	1.78	1.51		
	3000	3.42	2.36	2.69	1.99		
500	500	1.15	1.06	1.05	1.02	17.2	10.5
	1000	1.25	1.14	1.08	1.04	30.6	19.1
	1250	1.31	1.19	1.09	1.06	37.7	24.8
	2000	1.53	1.37	1.18	1.15		
	3000	1.9	1.67	1.37	1.34		

Table 2. Watson's results of relative photoelectron yield E_a using the same parameters as Table 1. a is the grain radius. L_e is the electron escape length. m is the index of refraction.

Graphite Yield Enhancement

$a=100 \text{ \AA}$

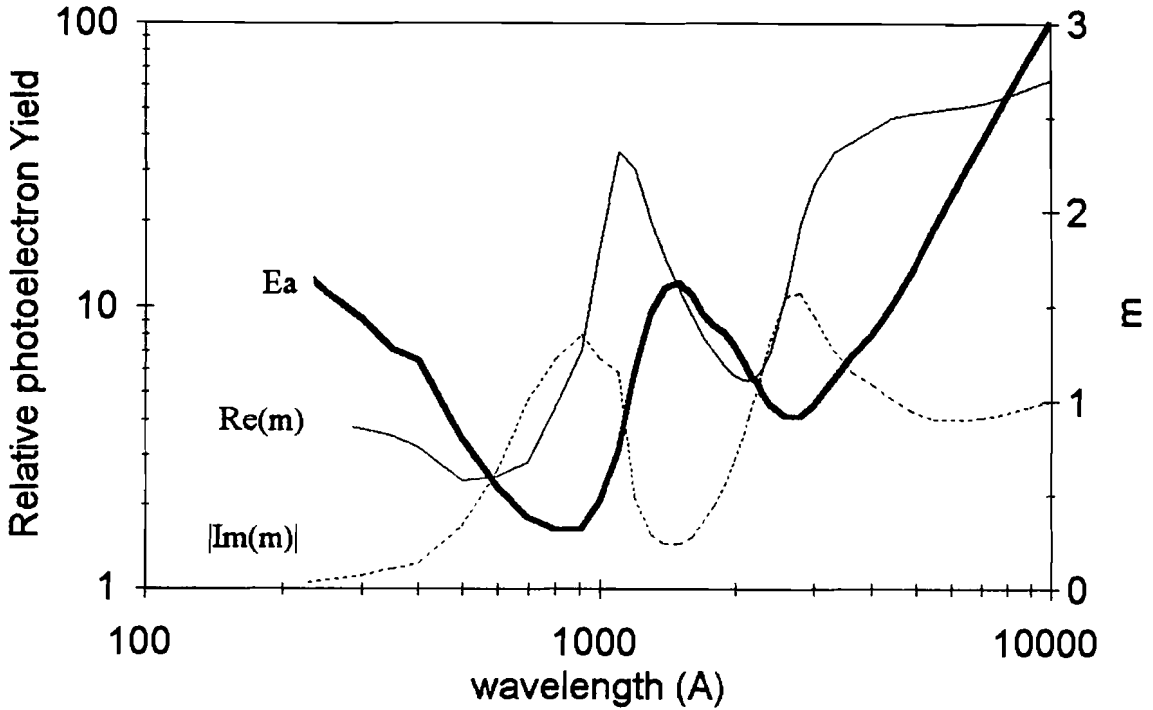


Figure 1. Graphite grains relative photoelectron yield E_a and complex index of refraction m vs wavelength. $Re(m)$ is the real part of m , $|Im(m)|$ is the value of the imaginary part of m . Radius of this dust grain is $a=100\text{\AA}$. Wavelength is from 227.9 \AA to 10000 \AA .

Graphite Yield Enhancement

$a=1000 \text{ \AA}$

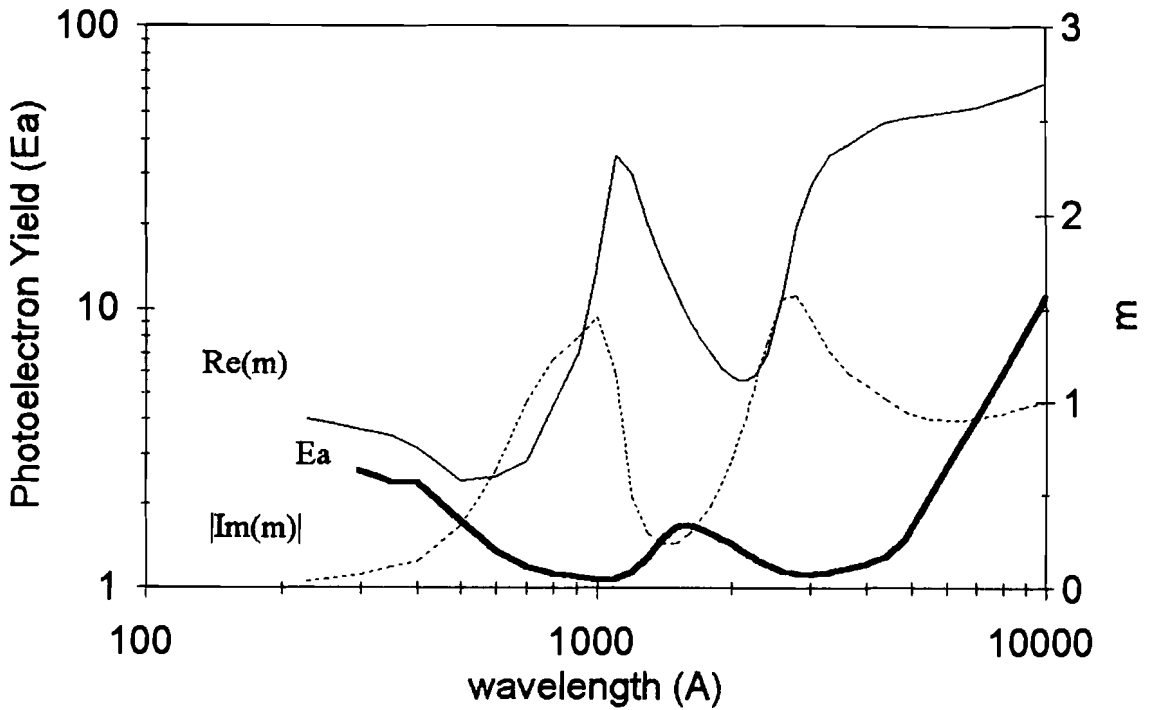


Figure 2. Graphite grains relative photoelectron yield E_a and complex index of refraction m vs wavelength. $Re(m)$ is the real part of m , $|Im(m)|$ is the value of the imaginary part of m . Radius of this dust grain is $a=1000\text{\AA}$. Wavelength is from 227.9\AA to 10000\AA .

Silicate Yield Enhancement

$a=1000 \text{ \AA}$

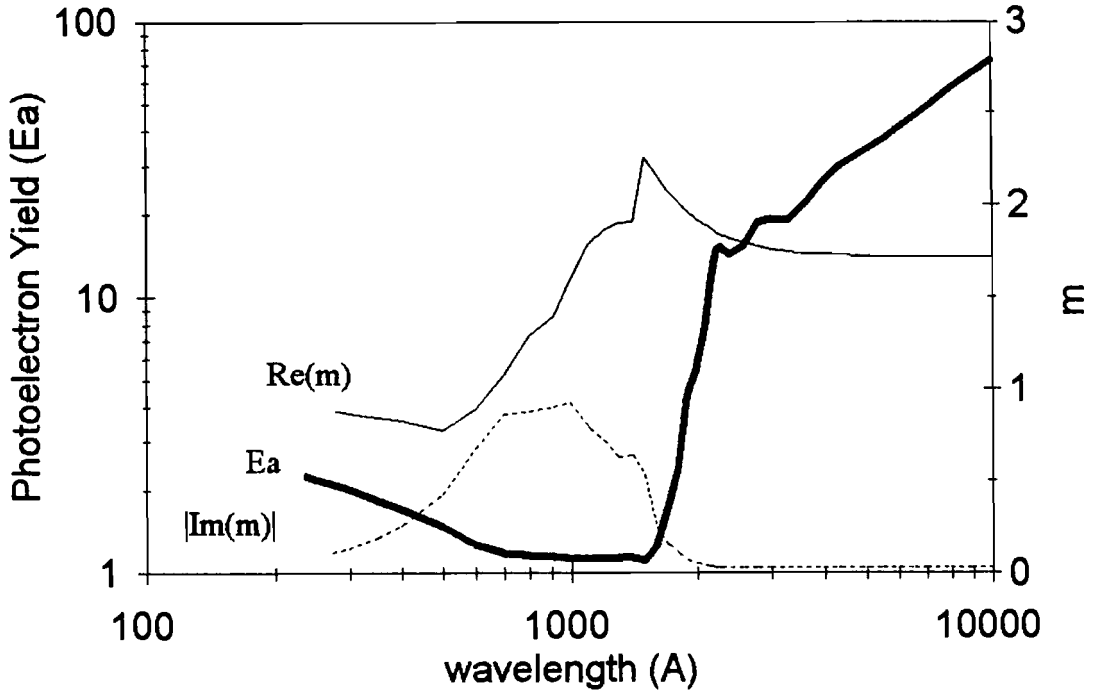


Figure 3. Silicate grains relative photoelectron yield E_a and complex index of refraction m vs wavelength. $Re(m)$ is the real part of m , $|Im(m)|$ is the value of the imaginary part of m . Radius of this dust grain is $a=1000\text{\AA}$. Wavelength is from 227.9\AA to 10000\AA .

Graphite Particle Yield

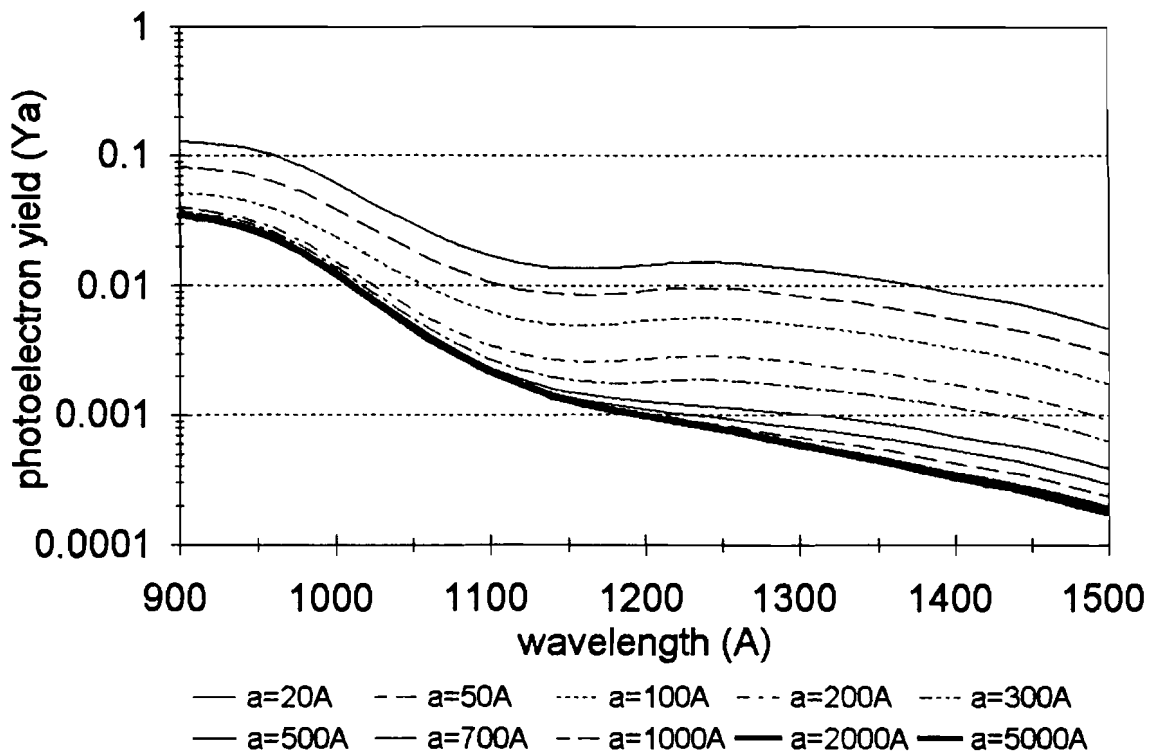


Figure 4. Various sizes of graphite dust grains absolute photoelectron yield Y_a vs wavelength. Grain sizes are from 20A to 5000A. Wavelength is from 900A to 1500A.

Silicate Particle Yield

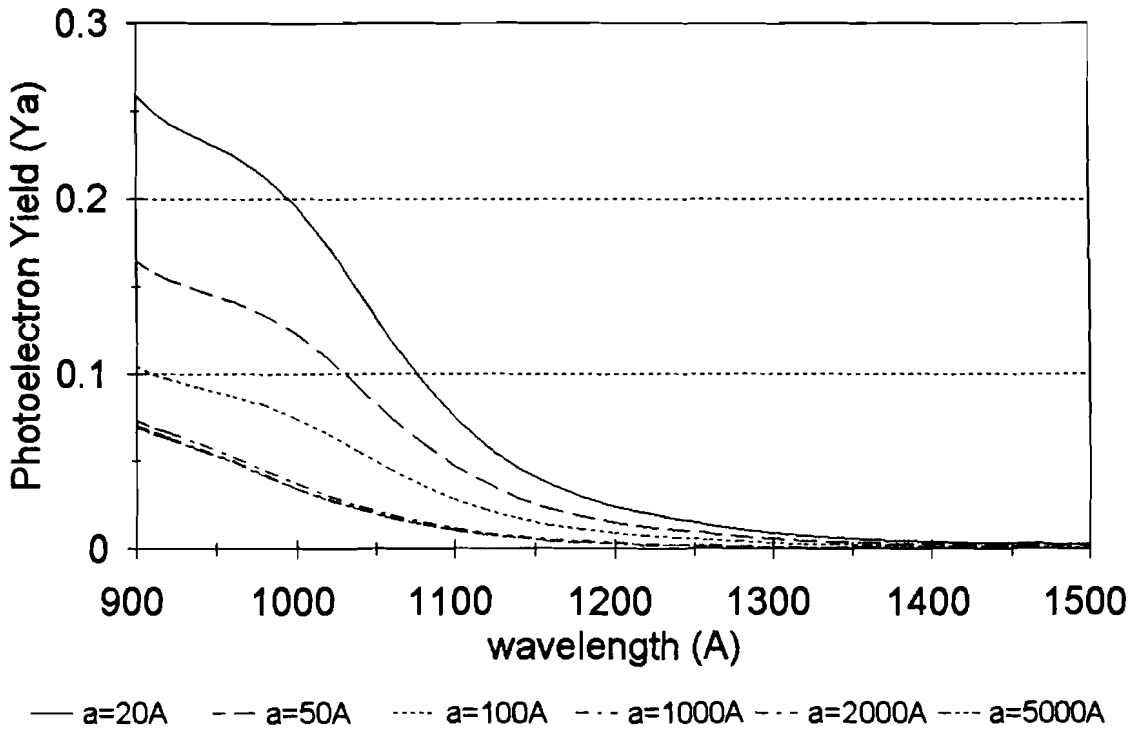


Figure 5. Various sizes of silicate dust grains absolute photoelectron yield Y_a vs wavelength. Grain sizes are from 20 \AA to 5000 \AA . Wavelength is from 900 \AA to 1500 \AA .

Chapter 4

Conclusions

This research has extended previous work by Shi.¹³ It investigated one of the mechanisms by which interstellar gas is heated and the emission of photoelectrons from graphite and silicate dust grains. It is found that grain size is important in the efficiency of photoelectron emission.

We have found that the relative photoelectron yield is always greater than one for both graphite and silicate grains. This confirms Watson's idea that enhanced photoemission from small dust grains can be significantly larger than bulk matter. We have reproduced Watson's numerical results and extended them.

This research presents the relationships of photoelectron yield, photon wavelength and grain size as well as the complex index of refraction. These relations are complicated and may be significant in the interstellar medium. More research, especially using a different model, may be necessary in the future. Ultimately, the photoelectron yields of known interstellar grains should be measured experimentally, although this will be a difficult task.

We have also discussed analytical and numerical methods in this thesis. It is clear that these numerical methods are powerful, and provide a useful general method for future study of the interaction of small grains with photons.

The absolute photoelectric yields calculated in this research will be

used in the future to calculate the number of photoelectrons emitted from small grains in different environments.

REFERENCES

1. C.F. Mckee and J.P. Ostriker, **Ap . J. , 218** 148. (1977).
 - 1.1. D C B Whittet, *Dust in the Galactic Environment*.(IOP, London) 1992.
 - 1.2. D.J. Hollenbach, **Ap.J. , 265**, 223 (1989).
2. W.D. Watson, **Ap . J. , 176**, 103 (1972); **J. Opt. Soc. Am.**, **63**,164 (1973).
3. W.W. Duley, **Ap. Space Sci. , 45**, 261 (1976).
4. B.T. Draine and H.M. Lee, **Ap . J. , 285**, 89 (1984).
5. C.F. Bohren and D.R. Huffman, *Absorption and Scattering of Light by Small Particles* (Wiley, New York, 1983).
6. S.V. Pepper, **J. Opt. Sco. Am. , 60**, 805 (1970).
7. J.D. Jackson, *Classical Electrodynamics* (Wiley, New York, 1962), p.65.
8. J.D. Jackson, *Classical Electrodynamics* (Wiley, New York, 1962), p.545.

9. H.C. van de Hulst, *Light Scattering by Small Particles* (Wiley, New York, 1957).
10. C.F. Bohren and D.R. Huffman, *Absorption and Scattering of Light by Small Particles* (Wiley, New York, 1983), p.127.
11. C.F. Bohren and D.R. Huffman, *Absorption and Scattering of Light by Small Particles* (Wiley, New York, 1983), p.87.
12. Frank Bowman, *Introduction to Bessel Functions* (Dover, New York, 1958).
13. Y. Shi, *Photoelectron Yield Enhancement in Interstellar Dust* unpublished report Emporia State University (1992).
- 13.5 J. Ballester, Y. Shi, and E. Dwek, *Photoelectron Yield of Silicate and Graphite Grains* manuscript (1994).
14. J. Wiscombe, **Appl. Opt.** , **19**, 1505 (1980).
15. C.F. Bohren and D.R. Huffman, *Absorption and Scattering of Light by Small Particles* (Wiley, New York, 1983). p. 100
16. H.C. van de Hulst, *Light Scattering by Small Particles* (Wiley, New York, 1957), p.123.
17. Personal communications from D. Alboth and W. Schneeberger

18. Wolfram Research, *Mathematica*
(Wolfram Research, Champaign, IL, 1991), Version 2.0

Appendix A

Exp($i\omega t$) and Exp($-i\omega t$) time-conventions

(1) exp($-i\omega t$) time-convention:

In Gaussian units, Maxwell equations can be written as

$$\begin{aligned}\nabla \times \vec{\mathbf{H}} &= \frac{4\pi}{c} \vec{\mathbf{I}} + \frac{1}{c} \frac{d\vec{\mathbf{D}}}{dt}, \\ \vec{\mathbf{D}} &= \epsilon \vec{\mathbf{E}}, \\ \nabla \times \vec{\mathbf{E}} &= -\frac{1}{c} \frac{d\vec{\mathbf{H}}}{dt}, \\ \text{div} \vec{\mathbf{I}} + \frac{d\rho}{dt} &= 0.\end{aligned}\tag{A1}$$

The boundary conditions are

$$\begin{aligned}\text{div} \vec{\mathbf{D}} &= 4\pi\rho, \\ \nabla \cdot \vec{\mathbf{H}} &= 0.\end{aligned}\tag{A2}$$

The electromagnetic wave field can be described

$$\vec{\mathbf{E}}(\vec{\mathbf{r}}, t) = \vec{\mathbf{E}}(\vec{\mathbf{r}}) e^{-i\omega t}$$

and

$$\vec{\mathbf{H}}(\vec{\mathbf{r}}, t) = \vec{\mathbf{H}}(\vec{\mathbf{r}})e^{-i\omega t}. \quad (\text{A3})$$

Substituting these electric field and magnetic fields into the Maxwell's equations, and using the electric field $\vec{\mathbf{E}}(\vec{\mathbf{r}}, t)$ to express the magnetic field $\vec{\mathbf{H}}(\vec{\mathbf{r}}, t)$, one obtains

$$\nabla \times \vec{\mathbf{H}} = -i \frac{\omega}{c} \left(\varepsilon + i \frac{4\pi\sigma}{\omega} \right) \vec{\mathbf{E}}. \quad (\text{A4})$$

Thus, two definitions are given as

$$m^2 = \varepsilon + i \frac{4\pi\sigma}{\omega} \quad (\text{A5})$$

$$k = \frac{\omega}{c},$$

where c is the speed of light, ω is the incident light's frequency. Then

$$\nabla \times \vec{\mathbf{H}} = -ikm^2 \vec{\mathbf{E}}. \quad (\text{A6})$$

Because

$$\begin{aligned} \nabla \cdot (\nabla \times \vec{\mathbf{H}}) &= 0, \\ \nabla \cdot (m^2 \vec{\mathbf{E}}) &= 0. \end{aligned} \quad (\text{A7})$$

On the other hand,

$$\nabla \times \vec{\mathbf{E}} = -\frac{1}{c} \frac{d\vec{\mathbf{H}}}{dt} = -\frac{1}{c} H(r) \frac{d}{dt}(-i\omega t) = ik\vec{\mathbf{H}}, \quad (\text{A8})$$

and from vector calculation formulas, one can obtain,

$$\nabla \times (\nabla \times \vec{\mathbf{E}}) = \nabla(\nabla \cdot \vec{\mathbf{E}}) - \nabla^2 \vec{\mathbf{E}} = -\nabla^2 \vec{\mathbf{E}}. \quad (\text{A9})$$

Thus

$$\nabla^2 \vec{\mathbf{E}} + k^2 m^2 \vec{\mathbf{E}} = 0. \quad (\text{A10})$$

This is the famous wave equation. Thus its scalar wave function is

$$\nabla^2 \psi + k^2 m^2 \psi = 0. \quad (\text{A11})$$

Here, ψ is a solution of this scalar wave equation. If two vectors $\vec{\mathbf{M}}, \vec{\mathbf{N}}$ are defined as,

$$\vec{\mathbf{M}} = \nabla \times (\vec{\mathbf{r}}\psi)$$

$$\vec{\mathbf{N}} = \frac{(\nabla \times \vec{\mathbf{M}})}{mk}, \quad (\text{A12})$$

then , the following expressions satisfy Maxwell equations,

$$\begin{aligned}\vec{\mathbf{E}} &= \vec{\mathbf{M}}_v + i\vec{\mathbf{N}}_u \\ \vec{\mathbf{H}} &= m(-\vec{\mathbf{M}}_u + i\vec{\mathbf{N}}_v).\end{aligned}\tag{A13}$$

From electromagnetic field boundary conditions, and change the Gauss unit to SI unit for simplify the equations, one can obtain,

$$\begin{aligned}j_n(mx)c_n + h_n^{(1)}(x)b_n &= j_n(x) \\ \mu[mxj_n(mx)]' c_n + \mu_1[xh_n^{(1)}(x)]' b_n &= \mu_1[xj_1(x)]' \\ \mu mj_n(mx)d_n + \mu_1h_n^{(1)}(x)a_n &= \mu_1j_n(x) \\ [mxj_n(mx)]' d_n + m[xh_n^{(1)}(x)]' a_n &= m[xj_n(x)].\end{aligned}\tag{A14}$$

These results can be found in the book written by Bohren & Huffman.¹⁵ But one must notice that, the unit used in Bohren & Huffman's book is SI Unit. Therefore, the form of wave equation in Bohren & Huffman is different from above discussion. In the case, $\mu = \mu_1$, one can solve these equations and obtain

$$c_n = \frac{j_n(x)[xh_n^{(1)}(x)]' - h_n^{(1)}(x)[xj_n(x)]'}{j_n(mx)[xh_n^{(1)}(x)]' - h_n^{(1)}(x)[mxj_n(mx)]'}\tag{A15}$$

$$\begin{aligned}
d_n &= \frac{mj_n(x)[xh_n^{(1)}(x)]' - mh_n^{(1)}(x)[xj_n(x)]'}{m^2 j_n(mx)[xh_n^{(1)}(x)]' - h_n^{(1)}(x)[mxj_n(mx)]'} \\
&= \frac{j_n(x)[xh_n^{(1)}(x)]' - h_n^{(1)}(x)[xj_n(x)]'}{mj_n(mx)[xh_n^{(1)}(x)]' - h_n^{(1)}(x)[xj_n(mx)]'}
\end{aligned} \tag{A16}$$

In order to separate m for $\exp(-i\omega t)$ and $\exp(i\omega t)$, from now on, m_+ and m_- are used to instead of m , then equations(14) and (15) can be written as,

$$c_n = \frac{j_n(x)[xh_n^{(1)}(x)]' - h_n^{(1)}(x)[xj_n(x)]'}{j_n(m_-x)[xh_n^{(1)}(x)]' - h_n^{(1)}(x)[m_-xj_n(m_-x)]'} \tag{A17}$$

$$d_n = \frac{m_-j_n(x)[xh_n^{(1)}(x)]' - h_n^{(1)}(x)[xj_n(x)]'}{m_-^2 j_n(m_-x)[xh_n^{(1)}(x)]' - h_n^{(1)}(x)[m_-xj_n(m_-x)]'} \tag{A18}$$

(2) $\exp(i\omega t)$ time-convention:

No matter what kind of time-convention, the Maxwell equations are the same form. However, the electromagnetic wave field in this case can be described as $\vec{\mathbf{E}}(\vec{\mathbf{r}}, t) = \vec{\mathbf{E}}(\vec{\mathbf{r}})e^{i\omega t}$, and $\vec{\mathbf{H}}(\vec{\mathbf{r}}, t) = \vec{\mathbf{H}}(\vec{\mathbf{r}})e^{i\omega t}$. Substituting these

electric field and magnetic fields into the Maxwell's equations, and using the electric field $\vec{\mathbf{E}}(\vec{r}, t)$ to express the magnetic field $\vec{\mathbf{H}}(\vec{r}, t)$, one obtains,

$$\nabla \times \vec{\mathbf{H}} = i \frac{\omega}{c} \left(\varepsilon - i \frac{4\pi\sigma}{\omega} \right) \vec{\mathbf{E}}. \quad (\text{A19})$$

Thus, two definitions are given as

$$m_+^2 = \varepsilon - i \frac{4\pi\sigma}{\omega} \quad (\text{A20})$$

$$k = \frac{\omega}{c},$$

where c is also the speed of light, ω is the incident light's frequency. Then

$$\nabla \times \vec{\mathbf{H}} = ikm_+^2 \vec{\mathbf{E}}. \quad (\text{A21})$$

Because

$$\nabla \cdot (\nabla \times \vec{\mathbf{H}}) = 0,$$

$$\nabla \cdot (m_+^2 \vec{\mathbf{E}}) = 0. \quad (\text{A22})$$

On the other hand,

$$\nabla \times \vec{\mathbf{E}} = -\frac{1}{c} \frac{d\vec{\mathbf{H}}}{dt} = -\frac{1}{c} \vec{\mathbf{H}}(r) \frac{d}{dt}(i\omega t) = -ik\vec{\mathbf{H}}, \quad (\text{A23})$$

and from vector calculation formulas, one can obtain,

$$\nabla \times (\nabla \times \vec{\mathbf{E}}) = \nabla(\nabla \cdot \vec{\mathbf{E}}) - \nabla^2 \vec{\mathbf{E}} = -\nabla^2 \vec{\mathbf{E}}. \quad (\text{A24})$$

Thus the same result as the $\exp(-i\omega t)$ time-convention is obtained

$$\nabla^2 \vec{\mathbf{E}} + k^2 m_+^2 \vec{\mathbf{E}} = 0. \quad (\text{A25})$$

Thus its scalar wave function is

$$\nabla^2 \psi + k^2 m_+^2 \psi = 0. \quad (\text{A26})$$

Similarity, ψ is a solution of this scalar wave equation, and two vectors $\vec{\mathbf{M}}, \vec{\mathbf{N}}$ are defined as,

$$\begin{aligned} \vec{\mathbf{M}} &= \nabla \times (\vec{\mathbf{r}} \psi) \\ \vec{\mathbf{N}} &= \frac{(\nabla \times \vec{\mathbf{M}})}{m_+ k}, \end{aligned} \quad (\text{A27})$$

then, the following expressions satisfy Maxwell equations,

$$\begin{aligned} \vec{\mathbf{E}} &= \vec{\mathbf{M}}_v + i\vec{\mathbf{N}}_u \\ \vec{\mathbf{H}} &= m_+ (-\vec{\mathbf{M}}_u + i\vec{\mathbf{N}}_v). \end{aligned} \quad (\text{A28})$$

From electromagnetic field boundary conditions, one can obtain¹⁶,

$$\Psi_n(x) - a_n \zeta_n(x) = m_+ c_n \Psi_n(y)$$

$$\Psi_n'(x) - a_n \zeta_n'(x) = c_n \Psi_n'(y)$$

$$\Psi_n(x) - b_n \zeta_n(x) = d_n \Psi_n(y)$$

$$\Psi_n'(x) - b_n \zeta_n'(x) = m_+ d_n \Psi_n'(y). \quad (\text{A29})$$

These results can be found in van de Hulst.⁹ Solving these equations, one obtains,

$$c_n = \frac{i}{\Psi_n'(y) \zeta_n(x) - m_+ \Psi(y) \zeta_n'(x)}$$

$$d_n = \frac{i}{m_+ \Psi_n'(y) \zeta_n(x) - \Psi_n(y) \zeta_n'(x)}, \quad (\text{A30})$$

where $y = m_+ x$, $x = ka$.

(3) The relations of c_n, d_n from $\exp(-i\omega t)$ and $\exp(i\omega t)$ time-conventions:

In order to make difference between these two cases, $c_n(+)$, $d_n(+)$ will be used to represent the results from $\exp(i\omega t)$ time term, $c_n(-)$, $d_n(-)$ will be used to represent the results from $\exp(-i\omega t)$ time term.

From the $\exp(-i\omega t)$ time-convention,

$$c_n(-) = \frac{j_n(x) \left[x h_n^{(1)}(x) \right]' - h_n^{(1)}(x) \left[x j_n(x) \right]'}{j_n(m_- x) \left[x h_n^{(1)}(x) \right]' - h_n^{(1)}(x) \left[m_- x j_n(m_- x) \right]'}, \quad (\text{A31})$$

because

$$\psi_n(x) = x j_n(x)$$

$$\zeta_n(x) = x h_n(x),$$

$$\Psi_n'(x) \zeta_n(x) - \Psi_n(x) \zeta_n'(x) = i \quad (\text{A32})$$

$c_n(-)$ can be written as

$$\begin{aligned} c_n(-) &= \frac{\frac{\Psi_n(x)}{x} \zeta_n^{(1)'}(x) - \frac{\zeta_n^{(1)}}{x} \Psi_n'(x)}{\frac{\Psi_n(m_- x)}{m_- x} \zeta_n^{(1)'}(x) - \frac{\zeta_n^{(1)}}{x} \Psi_n'(m_- x)} \\ &= \frac{\Psi_n(x) \zeta_n^{(1)'}(x) - \zeta_n^{(1)} \Psi_n'(x)}{\frac{\Psi_n(m_- x)}{m_-} \zeta_n^{(1)'}(x) - \zeta_n^{(1)} \Psi_n'(m_- x)} \\ &= \frac{-m_- i}{\Psi_n(m_- x) \zeta_n^{(1)'}(x) - m_- \zeta_n^{(1)} \Psi_n'(m_- x)}. \end{aligned}$$

$$= \frac{-m_+^* i}{\Psi_n(m_+^* x) \left[\zeta_n^{(2)'}(x) \right]^* - m_+^* \left[\zeta_n^{(2)} \right]^* \Psi_n'(m_+^* x)}. \quad (\text{A33})$$

Because , in $(i\omega t)$ time-convention:

$$\zeta_n^{(2)}(x) = x h_n^{(2)} = x [j_n(x) - iy_n(x)] \quad (\text{A34})$$

while in $(-i\omega t)$ time- convention:

$$\zeta_n^{(1)}(x) = x h_n^{(1)}(x) = x [j_n(x) + iy_n(x)]. \quad (\text{A35})$$

The relation of $\zeta_n^{(1)}(x)$ and $\zeta_n^{(2)}(x)$ is,

$$\zeta_n^{(1)}(x) = \left[\zeta_n^{(2)}(x) \right]^*. \quad (\text{A36})$$

The following relationship for a function of a complex variable will be useful.

$$\Psi_n(z^*) = \left[\Psi_n(z) \right]^* \quad (\text{A37})$$

This is not true in general, but is true for functions which are real for real arguments, for example polynomials with real coefficients. This property is known as the Schwarz Reflection Principle¹⁷. The Bessel functions and all

functions derived from them satisfy this condition. The relationship was also checked with the Mathematica¹⁸ computer algebra software.

Thus

$$c_n(-) = \left[\frac{-m_+ i}{\Psi_n(m_+ x) \zeta_n^{(2)'}(x) - m_+ \zeta_n^{(2)} \Psi_n'(m_+ x)} \right]^* . \quad (\text{A38})$$

On the other hand, from above calculation,

$$\begin{aligned} d_n(-) &= \frac{j_n(x) [xh_n^{(1)}(x)]' - h_n^{(1)}(x) [xj_n(x)]'}{m_- j_n(m_- x) [xh_n^{(1)}(x)]' - h_n^{(1)}(x) [xj_n(m_- x)]'} \\ &= \frac{j_n(x) \left\{ [xh_n^{(2)}(x)]' \right\}^* - [h_n^{(2)}(x)]^* [xj_n(x)]'}{(m_+^*) j_n(m_+^* x) \left\{ [xh_n^{(2)}(x)]' \right\}^* - [h_n^{(2)}(x)]^* [xj_n(m_+^* x)]'} \\ &= \frac{\left\{ j_n(x) \left\{ [xh_n^{(2)}(x)]' \right\} - [h_n^{(2)}(x)] [xj_n(x)]' \right\}^*}{\left\{ (m_+) j_n(m_+ x) \left\{ [xh_n^{(2)}(x)]' \right\} - [h_n^{(2)}(x)] [xj_n(m_+ x)]' \right\}^*} \\ &= \frac{\left\{ j_n(x) \left\{ [xh_n^{(2)}(x)]' \right\} - [h_n^{(2)}(x)] [xj_n(x)]' \right\}^*}{\left\{ (m_+) j_n(m_+ x) \left\{ [xh_n^{(2)}(x)]' \right\} - [h_n^{(2)}(x)] [xj_n(m_+ x)]' \right\}^*} \end{aligned}$$

$$\begin{aligned}
&= \frac{\left\{ j_n(x) \left\{ [x h_n^{(2)}(x)]' \right\} - [h_n^{(2)}(x)] [x j_n(x)]' \right\}^*}{\left\{ (m_+) j_n(m_+x) \left\{ [x h_n^{(2)}(x)]' \right\} - [h_n^{(2)}(x)] [x j_n(m_+x)]' \right\}^*} \\
&= \left\{ \frac{\frac{\Psi_n(x)}{x} \zeta_n'(x) - \frac{\zeta_n(x)}{x} \Psi_n'(x)}{\frac{\Psi_n(m_+x)}{x} \zeta_n^{(2)'}(x) - \frac{\zeta_n^{(2)}(x)}{m_+x} \Psi_n'(m_+x)} \right\}^* \\
&= \left[\frac{m_+ [\Psi_n(x) \zeta_n'(x) - \Psi_n'(x) \zeta_n(x)]}{m_+ \Psi_n(m_+x) \zeta_n^{(2)'}(x) - \zeta_n^{(2)}(x) \Psi_n'(m_+x)} \right]^* \quad (\text{A39}) \\
&= \left[\frac{m_+ i}{m_+ \Psi_n(m_+x) \zeta_n^{(2)'}(x) - \zeta_n^{(2)}(x) \Psi_n'(m_+x)} \right]
\end{aligned}$$

Thus

$$d_n(-) = \left[\frac{m_+ i}{m_+ \Psi_n(m_+x) \zeta_n^{(2)'}(x) - \zeta_n^{(2)}(x) \Psi_n'(m_+x)} \right]^* \quad (\text{A40})$$

From above $\exp(i\omega t)$ time-convention

$$c_n(+) = \frac{i}{\Psi_n'(m_+x) \zeta_n^{(2)}(x) - m_+ \Psi(m_+x) \zeta_n^{(2)'}(x)}$$

$$d_n(+)=\frac{i}{m_+\Psi_n'(m_+x)\zeta_n^{(2)}(x)-\Psi_n(m_+x)\zeta_n^{(2)'}(x)}, \quad (\text{A41})$$

equation(A6) and (A7) can be written as

$$c_n(-)=\left[\frac{-m_+i}{\Psi_n(m_+x)\zeta_n^{(2)'}(x)-m_+\zeta_n^{(2)}(x)\Psi_n'(m_+x)}\right]^* \\ =-m_+^*d_n^*(+) \quad (\text{A42})$$

that is

$$c_n(-)=-m_+^*d_n^*(+). \quad (\text{A43})$$

Similarity,

$$d_n(-)=\left[\frac{m_+i}{m_+\Psi_n(m_+x)\zeta_n^{(2)'}(x)-\zeta_n^{(2)}(x)\Psi_n'(m_+x)}\right]^* \\ =-m_+^*c_n^*(+) \quad (\text{A44})$$

thus

$$d_n(-)=-m_+^*c_n^*(+) \quad (\text{A45})$$

(4) The relative photoelectron yield Y'/Y_b :

From equation(28), the relative photoelectron yield can be written as

$$\frac{Y'}{Y_b} = \frac{(L_e + L_a) \int_0^a e^{-(a-r)/L_e} \left[\int_0^{4\pi} (\vec{M}_v^* \cdot \vec{M}_v + \vec{N}_u^* \cdot \vec{N}_u) d\Omega \right] r^2 dr}{L_e \int_0^a \left[\int_0^{4\pi} (\vec{M}_v^* \cdot \vec{M}_v + \vec{N}_u^* \cdot \vec{N}_u) d\Omega \right] r^2 dr} \quad (\text{A46})$$

where²

$$\begin{pmatrix} \vec{M}_u \\ \vec{M}_v \end{pmatrix} = \nabla \times \begin{pmatrix} \vec{r}u \\ \vec{r}v \end{pmatrix}.$$

in the $\exp(i\omega t)$ time-convention, but

$$\begin{pmatrix} \vec{M}_e \\ \vec{M}_o \end{pmatrix} = \nabla \times \begin{pmatrix} \vec{r}u \\ \vec{r}v \end{pmatrix}$$

in the $\exp(i\omega t)$ time-convention. Therefore the relative photoelectron yield in the $\exp(-i\omega t)$ time -convention can be written as

$$\frac{Y'}{Y_b} = \frac{(L_e + L_a) \int_0^a e^{-(a-r)/L_e} \left[\int_0^{4\pi} (\vec{M}_o^* \cdot \vec{M}_o + \vec{N}_e^* \cdot \vec{N}_e) d\Omega \right] r^2 dr}{L_e \int_0^a \left[\int_0^{4\pi} (\vec{M}_o^* \cdot \vec{M}_o + \vec{N}_e^* \cdot \vec{N}_e) d\Omega \right] r^2 dr}. \quad (\text{A47})$$

Because

$$\int_0^{4\pi} \vec{M}_o^* \cdot \vec{M}_o d\Omega = 4\pi |m_-|^2 \sum_{n=1}^{\infty} |d_n(-)|^2 (2n+1) j_n^*(m_- kr) \cdot j_n(m_- kr)$$

$$\begin{aligned}
&= 4\pi |m|^4 \sum_{n=1}^{\infty} |c_n(+)|^2 (2n+1) j_n(m_+ kr) \cdot j_n^*(m_+ kr) \\
&= |m|^2 \int_0^{4\pi} \tilde{\mathbf{M}}_v^* \cdot \tilde{\mathbf{M}}_v d\Omega
\end{aligned} \tag{A48}$$

Similarly, it is easy to show that

$$\int_0^{4\pi} \tilde{\mathbf{N}}_e^* \cdot \tilde{\mathbf{N}}_e d\Omega = |m|^2 \int_0^{4\pi} \tilde{\mathbf{N}}_u^* \cdot \tilde{\mathbf{N}}_u d\Omega. \tag{A49}$$

Using the $c_n(+)$, $d_n(+)$ to express the above equation, that is

$$\begin{aligned}
\frac{Y'}{Y_b} &= \frac{(L_e + L_a) \int_0^q e^{-(a-r)/L_e} \left[\int_0^{4\pi} (\tilde{\mathbf{M}}_o^* \cdot \tilde{\mathbf{M}}_o + \tilde{\mathbf{N}}_e^* \cdot \tilde{\mathbf{N}}_e) d\Omega \right] r^2 dr}{L_e \int_0^q \left[\int_0^{4\pi} (\tilde{\mathbf{M}}_o^* \cdot \tilde{\mathbf{M}}_o + \tilde{\mathbf{N}}_e^* \cdot \tilde{\mathbf{N}}_e) d\Omega \right] r^2 dr} \\
&= \frac{(L_e + L_a) \int_0^q e^{-(a-r)/L_e} |m|^2 \left[\int_0^{4\pi} (\tilde{\mathbf{M}}_v^* \cdot \tilde{\mathbf{M}}_v + \tilde{\mathbf{N}}_u^* \cdot \tilde{\mathbf{N}}_u) d\Omega \right] r^2 dr}{L_e \int_0^q |m|^2 \left[\int_0^{4\pi} (\tilde{\mathbf{M}}_v^* \cdot \tilde{\mathbf{M}}_v + \tilde{\mathbf{N}}_u^* \cdot \tilde{\mathbf{N}}_u) d\Omega \right] r^2 dr}
\end{aligned}$$

$$= \frac{(L_e + L_a) \int_0^a e^{-(a-r)/L_e} \left[\int_0^{4\pi} (\bar{\mathbf{M}}_v^* \cdot \bar{\mathbf{M}}_v + \bar{\mathbf{N}}_u^* \cdot \bar{\mathbf{N}}_u) d\Omega \right] r^2 dr}{L_e \int_0^a \left[\int_0^{4\pi} (\bar{\mathbf{M}}_v^* \cdot \bar{\mathbf{M}}_v + \bar{\mathbf{N}}_u^* \cdot \bar{\mathbf{N}}_u) d\Omega \right] r^2 dr} \quad (\text{A50})$$

Equation (A24) and equation(28) are equal. It is clear that the final result of relative photoelectron yield is the same no matter in what kind of time-conventions. That means that even though the results for c_n and d_n will change with the time-convention, the final result of photoelectron yield will be the same. It is not dependent on the time-convention.

Appendix B

The emission of photoelectron from dust grains is perhaps the most important heating mechanism of the interstellar gas. If the energy of the ejected photoelectrons is more than the energy of the electrons which are absorbed, then there is a net heating of the surrounding gas. In order to reduce the uncertainty in the photoelectron yield of small grains as much as possible, the absorption efficiency Q_{abs} must be evaluated. The following is an example which uses the photoelectron yield Y_p that has been calculated from the computer program PE-DING.

Generally speaking electrons are strongly bound in a solid but those of highest energy may overcome the surface potential barrier. For a given material, this process only occurs for photons having energy greater than the work function

$$\phi = h\nu_1. \quad (\text{B1})$$

The energy E of the ejected photoelectron depends on the energy of the incident photon via

$$E = h\nu - h\nu_1. \quad (\text{B2})$$

If a is the spherical grain's radius, then the cross-section for the absorption of radiation is given by $\pi a^2 Q_{abs}$.

Not every absorbed photon gives rise to a photoelectron. It depends on the photoelectron yield Y_p . If the grain is situated a distance r from a source of radiation of luminosity L_ν , the flux density at frequency ν at the grain is

$$\frac{L_\nu}{4\pi r^2}. \quad (\text{B3})$$

However, the most important quantity is the number of photons being intercepted by the grain. Thus, the number of photons in the frequency range $\nu \rightarrow \nu + d\nu$ arriving at the grain is

$$\frac{L_\nu}{4\pi r^2 h \nu} d\nu. \quad (\text{B4})$$

Then the total rate at which photoelectrons are emitted is

$$\int_{\phi_{eff}}^{\infty} \frac{L_\nu}{4\pi r^2 h \nu} Y_p \pi a^2 Q_{abs} d\nu. \quad (\text{B5})$$

If the grain is positively charged, it becomes more difficult for the electrons to escape from the grain: the Coulomb attraction between grain and electron effectively increases the photoelectric work function of radius a by an amount given by

$$\frac{Ze^2}{4\pi\epsilon_0 a}, \quad (\text{B6})$$

where Ze is the positive charge on the grain. Therefore the work function in this case can be written as

$$\phi_{eff} = h\nu_1 + \frac{Ze^2}{4\pi\epsilon_0 a}. \quad (\text{B7})$$

The absorption efficiency Q_{abs} can be obtained from FORTRAN program. The energy L_ν can be obtained from Planck formula and some other descriptions. Future study will be done in this area.

Appendix C

```
*****
* -PROGRAM: PE_DING.FOR *
* * *
* -AUTHOR: Yu Shi *
* -DATES: May 1, 1992 *
* * *
* -LAST MODIFIED BY: Jorge Ballester and Yihong Ding *
* -DATE: February 18, 1994 *
* * *
* -DESCRIPTION: Calculates the photoyield enhancement y'/y *
* for a given sphere refractive index, medium *
* refractive index, radius, and free space *
* wavelength. *
* * *
* -NOTES: Input format has been changed! *
*****
*
IMPLICIT DOUBLE PRECISION (A-H,O-Z)
COMMON/BLCK0/C(500),E(500)
COMMON/BLCK1/X,Y,NSTOP
COMMON/BLCK2/ WAVEL,REFREL,REFMED,RAD
COMMON/BLCK3/ A,B,KQ,ESCPL
COMPLEX REFREL
COMPLEX Y
COMPLEX C,E
PARAMETER (PI=3.14159265, TOL=1.0D-4, DEPTH=10)
DATA ESCPL,REFMED/10,1.0/
WRITE(6,*)'THIS IS PE_DING!'
WRITE(6,*)'DEPTH=',DEPTH

*****
* Input real refractive index for surrounding medium REFMED. *
*****
*option WRITE(6,*) 'REFMED='
*option READ(5,*) REFMED
*
* Open input and output files.
OPEN(10,file='radius.dat',status='old')
OPEN(16,file='refindx.dat',status='old')
OPEN(20,file='pe-out',status='unknown')
*
```

```

*****
* Input escape length (ESCPL) and radius (RAD) in angstroms.          *
*****

*****
* Input from keyboard with the following statements.                    *
*option  WRITE(6,*)RADIUS='                                           *
*option  READ(5,*) RAD                                                 *
*option  WRITE(6,*)'ESCAPE LENGTH='                                     *
*option  READ(5,*) ESCPL                                              *
*****
*
*
* Read radius (RAD) from input file. Return to label 30 after calculating
* yield enhancement for all photon wavelengths (fixed radius).
30 READ(10,*,END=160)RAD
   WRITE(6,*)'RAD=',RAD
   WRITE(20,*)'RAD=',RAD
   WRITE(20,*)'DEPTH=',DEPTH
*
* Read wavelength (WAVEL) in Angstroms, and complex refractive
* index (REFRE,REFIM) from input file. Return to label 40
* after calculating yield enhancement for each wavelength.
40 READ(16,*,END=140)WAVEL,REFRE,REFIM
*
*****
* Input from keyboard with the following statements.                    *
*option  WRITE(6,*)'WAVELENGTH='                                       *
*option  READ(5,*) WAVEL                                               *
*option  WRITE(6,*)'REFRE=',REFIM='                                   *
*option  READ(5,*) REFRE,REFIM                                         *
*****
REFREL=CMPLX(REFRE,REFIM)/REFMED
X=2.*PI*RAD*REFMED/WAVEL
Y=X*REFREL
*
* Calculate the photon absorption length ALENGTH.
ALENGTH=WAVEL/(4.*PI*ABS(REFIM))
*
* Determine number of terms in series (NSTOP).
XSTOP=ABS(Y)+4.*(ABS(Y))**(1./3.)+2.0
*option  NSTOP=XSTOP
NSTOP=1
TEMP=0

```

```

DO 77 JI=0,50
*option      NSTOP=NSTOP+1
             NSTOP=1.5*NSTOP+1
* Call the coefficients c_n and d_n.
  CALL COEFL(C,E)
*
* Input lower limit A and upper limit B for radial integrals.
* A cannot equal 0 but can be a very small number.
*option      A=.001
             B=RAD
*
* Use the flag KQ to calculate the numerator (KQ=0),
* or the denominator (KQ=1).

      A=0.001
      KQ=0
      CALL INTEGRA(S)
      DENOMINATOR=S
      A=MAX(0.001,RAD-DEPTH*ESCPL)
      KQ=1
      CALL INTEGRA(S)
      OMINATOR=S
      YIELD=OMINATOR/DENOMINATOR
      YIELD=(ESCPL+ALENGTH)*YIELD/ESCPL
      WRITE(6,*)NSTOP,YIELD

*
* Check for convergence, if reached, exit loop.
      IF (ABS(YIELD-TEMP).LT.ABS(TEMP)*TOL) GOTO 70
      TEMP=YIELD
77 CONTINUE
      WRITE(6,*)'need to sum more terms'
      STOP
*
70 WRITE(6,848)NSTOP,WAVEL,YIELD
*
* Write to output file.
      WRITE(20,858)WAVEL,YIELD
*
* Return to read next wavelength.
      GOTO 40
*
140 CONTINUE
* Finished with list of wavelengths.

```



```

* Rewind to the beginning of wavelengths.
  REWIND 16
*
* Return to read next radius.
  GOTO 30
*
160 CONTINUE
* Finished with list of radii.
* Close files.
  CLOSE(10,status='keep')
  CLOSE(16,status='keep')
  CLOSE(20,status='keep')
*
858 FORMAT(f12.4,f14.4)
848 FORMAT('1YIELD(',I3,')=',F10.4,10x,F10.4)
*
  STOP
  END

*****
* Compute the coefficients c_n, d_n. *
*****

SUBROUTINE COEFL(C,E)
IMPLICIT DOUBLE PRECISION(A-H,O-Z)
COMMON/BLCK1/X,Y,NSTOP
COMMON/BLCK2/WAVEL,REFREL,REFMED,RAD
COMPLEX XI,XI1,D(500),C(500),E(500)
COMPLEX I,CPSI(500),COMX,Y
COMPLEX REFREL
DOUBLE PRECISION RBESSJ(500)
YMOD=ABS(Y)
NMX=MAX(NSTOP,INT(YMOD))+15
*****

* Calculate the logarithmic derivative D_n. *
*****

CALL DERIV(NMX,D,Y)
I=CMPLX(0.0,1.0)
ZERO=0.0
COMX=CMPLX(X,ZERO)
*****

* Call subroutines to compute Riccati-Bessel function with *
* complex and real arguments (only for PSI function) *
*****

CALL BESSJR(NSTOP+1,X,RBESSJ)
CALL BESSJ(NSTOP+1,Y,CPSI)

```

```

PSI1=SIN(X)
CHI0=-SIN(X)
CHI1=COS(X)
XI1=CMPLX(PSI1,CHI1)
DO 777 N=1,NSTOP
  RN=N
  DN=N
  PSI=RBESSJ(N+1)

```

```

*****
* Calculate XI function using upward recurrence method. *
*****

```

```

  CHI=(2.*DN-1.)*CHI1/X-CHI0
  XI=CMPLX(PSI,CHI)
  E(N)=((REFREL*D(N)+RN/X)*XI-XI1)*CPSI(N+1)
  E(N)=I/E(N)
  C(N)=((D(N)+REFREL*RN/X)*XI-REFREL*XI1)*CPSI(N+1)
  C(N)=I/C(N)
  CHI0=CHI1
  CHI1=CHI
  XI1=XI
777 CONTINUE
  RETURN
  END

```

```

*****
* Perform integrations. *
* Adapted from 'Numerical Recipes' by Press, et. al. *
*****

```

```

SUBROUTINE INTEGRA(S)
  IMPLICIT DOUBLE PRECISION(A-H,O-Z)
  COMMON/BLCK0/C(500),E(500)
  COMMON/BLCK1/X,Y,NSTOP
  COMMON/BLCK2/WAVEL,REFREL,REFMED,RAD
  COMMON/BLCK3/A,B,KQ,ESCPL
  COMPLEX C,E
  PARAMETER (EPS=1.E-6,JMAX=20)
  OST=-1.E30
  OS=-1.E30
  DO 11 J=1,JMAX
    CALL TRAPZED(ST,J)
    S=(4.*ST-OST)/3.
    IF (ABS(S-OS).LT.EPS*ABS(OS)) RETURN
    OS=S
    OST=ST

```

```

11 CONTINUE
  PAUSE 'too many steps'
  END

```

```

SUBROUTINE TRAPZED(S,N)
  IMPLICIT DOUBLE PRECISION(A-H,O-Z)
  COMMON/BLCK0/C(500),E(500)
  COMMON/BLCK1/ X,Y,NSTOP
  COMMON/BLCK2/WAVEL,REFREL,REFMED,RAD
  COMMON/BLCK3/A,B,KQ,ESCPL
  DO 33 K=1,NSTOP

```

```

33 CONTINUE
  IF (N.EQ.1) THEN
    S=.5*(B-A)*(BFUNC(A)+BFUNC(B))
    IT=1
  ELSE
    TNM=IT
    DEL=(B-A)/TNM
    XX=A+.5*DEL
    SUM=0
    DO 11 J=1,IT
      SUM=SUM+BFUNC(XX)
      XX=XX+DEL

```

```

11 CONTINUE
  S=.5*(S+(B-A)*SUM/TNM)
  IT=2*IT
  END IF
  RETURN
  END

```

```

*****
* Compute F(r). *
*****

```

```

FUNCTION BFUNC(R)
  IMPLICIT DOUBLE PRECISION(A-H,O-Z)
  COMMON/BLCK0/C(500),E(500)
  COMMON/BLCK1/X,Y,NSTOP
  COMMON/BLCK2/WAVEL,REFREL,REFMED,RAD
  COMMON/BLCK3/A,B,KQ,ESCPL
  COMPLEX Z,DZ,ZPSI(500),zdn(500)
  COMPLEX C,E,REFREL
  DOUBLE PRECISION NN,MM,K,mn

```

```

mn=0.0
NN=0.0
MM=0.0
K=2.*3.1415926*REFMED/WAVEL
Z=K*R*REFREL
DZ=Z

```

```

*****
* Calculate Riccati-Bessel function with complex argument (mkr) *
*****

```

```

CALL BESSJ(NSTOP+1,DZ,ZPSI)
NAN=NSTOP+15
CALL DERIV(NAN,ZDN,Z)
DO 888 N=NSTOP,1,-1
RN=N
mn=mn+(2.*rn+1.)*(abs(zpsi(n+1)))**2.*
$ ((abs(c(n)))**2.*(abs(zdn(n)))**2.+
$ (abs(e(n)))**2.+rn*(rn+1.)*(abs(c(n)))**2.
$ /((abs(z))**2.))

```

```

*****

```

```

* The following program is another way to computer F(r) *

```

```

*
* MM=MM+(ABS(E(N)))**2.*(2.*RN+1.)*
* $ (ABS(ZPSI(N+1)))**2./(K**2.)
* NN=NN+(ABS(C(N)))**2.*(2.*RN+1.)*
* $ ((ABS(ZPSI(N)-ZPSI(N+1)*RN/(REFREL*K*R)))**2.
* $ /(K**2.)
* $ +RN*(RN+1.)*(ABS(ZPSI(N+1)))**2.
* $ /((ABS(REFREL))**2.*(K**4.
* $ *R**2.))

```

```

*****

```

```

*

```

```

888 CONTINUE
IF(KQ.NE.0)THEN
  BFUNC=(mn)*EXP((R-RAD)/ESCPL)
ELSE
  BFUNC=mn
ENDIF
RETURN
END

```

```
*****
* Calculate Riccati-Bessel function with complex arguments *
* using downward recurrence. Adapted from 'Numerical Recipes.' *
*****
```

```

SUBROUTINE BESSJ(N,Y, RBESSJ)
COMPLEX Y,BJM,BJ,BJP,BESJO
COMPLEX RBESSJ(500),RATO
PARAMETER( IACC=40,BIGNO=1.E20,BIGNI=1.E-20)
YMOD=ABS(Y)
RBESSJ(1)=SIN(Y)
BESJO=SIN(Y)
M=2*((N+INT(SQRT(FLOAT(IACC*N))))/2)
BJP=CMPLX(0,0)
BJ=CMPLX(1,0)
DO 12 J=M,1,-1
    BJM=((2*J+1)*BJ)/Y-BJP
    BJP=BJ
    BJ=BJM

```

```

*
    IF(ABS(BJ).GT.BIGNO) THEN

```

```

* Renormalize to prevent overflows.
*

```

```

    BJ=BJ*BIGNI
    BJP=BJP*BIGNI
    BJM=BJM*BIGNI
    DO 555 ID=J+2,N
        RBESSJ(ID)=RBESSJ(ID)*BIGNI
555 CONTINUE
    ENDIF
    RBESSJ(J+1)=BJP
12 CONTINUE

```

```

*
* Normalize the results.
*

```

```

    RATO=BESJO/BJM
    DO 44 JJ=2,N
        RBESSJ(JJ)=RBESSJ(JJ)*RATO
44 CONTINUE
    END

```

```

SUBROUTINE DERIV(NMX,D,VAR)

```

```
*****
* Calculate the logarithmic derivative D(J) by downward *
* recurrence beginning with initial value 0.0 + 0.0*i at J=NMX. *
*****
```

```
IMPLICIT DOUBLE PRECISION(A-H,O-Z)
COMPLEX D(500),VAR
D(NMX)=CMPLX(0.0,0.0)
NN=NMX-1
DO 120 N=1,NN
RN=NMX-N+1
120 D(NMX-N)=(RN/VAR)-(1./(D(NMX-N+1)+RN/VAR))
RETURN
END
```

```
*****
* Calculate the Riccati-Bessel function with real functions. *
*****
```

```
SUBROUTINE BESSJR(N,Y,RBESSJ)
```

```
*****
* CALCULATE THE RICCATI-BESSEL USING DOWNWARD RECURRENCE *
*****
```

```
DOUBLE PRECISION Y,BJM,BJ,BJP,BESJO
DOUBLE PRECISION RBESSJ(500),RATO
PARAMETER(IACC=40,BIGNO=1.E20,BIGNI=1.E-20)
RBESSJ(1)=SIN(Y)
BESJO=SIN(Y)
M=2*((N+INT(SQRT(FLOAT(IACC*N))))/2)
BJP=CMPLX(0,0)
BJ=CMPLX(1,0)
DO 12 J=M,1,-1
BJM=((2*J+1)*BJ)/Y-BJP
BJP=BJ
BJ=BJM
IF(ABS(BJ).GT.BIGNO) THEN
```

```
*
* Renormalize to prevent overflows.
*
```

```
BJ=BJ*BIGNI
BJP=BJP*BIGNI
BJM=BJM*BIGNI
DO 555 ID=J+2,N
RBESSJ(ID)=RBESSJ(ID)*BIGNI
```

```
555 CONTINUE
ENDIF
```

```
        RBESSJ(J+1)=BJP
12 CONTINUE
*
* Normalize the results.NORMALIZE THE RESULTS
*
        RATO=BESJO/BJM
        DO 44 JJ=2,N
            RBESSJ(JJ)=RBESSJ(JJ)*RATO
44 CONTINUE
        END
```

I, Yihong Ding, hereby submit this thesis to Emporia State University as partial fulfillment of the requirements for an advanced degree. I agree that the Library of the University may make it available for use in accordance with its regulations governing materials of this type. I further agree that quoting, photocopying, or other reproduction of this document is allowed for private study, scholarship (including teaching) and research purposes of a nonprofit nature. No copying which involves potential financial gain will be allowed without written permission of the author.

Yihong Ding
Signature of Author

July 29, 1994
Date

Photoelectron Yield Enhancement of
Small Graphite and Silicate Dust Grains
Title of Thesis

Way Cooper
Signature of Graduate Office
Staff Member

July 27, 1994
Date Received

1
P.S.